Chemistry & Biology 13, 1041–1050, October 2006 DOI 10.1016/j.chembiol.2006.08.008

An Enzyme that Regulates Ether Lipid Signaling Pathways in Cancer Annotated by Multidimensional Profiling

Kyle P. Chiang,[1,2] Sherry Niessen,[1,2] Alan Saghatelian,[1] and Benjamin F. Cravatt[1,*]
[1]The Skaggs Institute for Chemical Biology and Departments of Cell Biology and Chemistry
The Scripps Research Institute
10550 North Torrey Pines Road
La Jolla, California 92037

Summary

Hundreds, if not thousands, of uncharacterized enzymes currently populate the human proteome. Assembly of these proteins into the metabolic and signaling pathways that govern cell physiology and pathology constitutes a grand experimental challenge. Here, we address this problem by using a multidimensional profiling strategy that combines activity-based proteomics and metabolomics. This approach determined that KIAA1363, an uncharacterized enzyme highly elevated in aggressive cancer cells, serves as a central node in an ether lipid signaling network that bridges platelet-activating factor and lysophosphatidic acid. Biochemical studies confirmed that KIAA1363 regulates this pathway by hydrolyzing the metabolic intermediate 2-acetyl monoalkylglycerol. Inactivation of KIAA1363 disrupted ether lipid metabolism in cancer cells and impaired cell migration and tumor growth in vivo. The integrated molecular profiling method described herein should facilitate the functional annotation of metabolic enzymes in any living system.

Introduction

Elucidation of the metabolic and signaling networks that regulate health and disease stands as a principal goal of postgenomic research. The remarkable complexity of these molecular pathways has inspired the advancement of "systems biology" methods for their characterization [1]. Toward this end, global profiling technologies, such as DNA microarrays [2, 3] and mass spectrometry (MS)-based proteomics [4, 5], have succeeded in generating gene and protein signatures that depict key features of many human diseases. However, extricating from these associative relationships the roles that specific biomolecules play in cell physiology and pathology remains problematic, especially for proteins of unknown biochemical or cellular function.

The functions of certain proteins, such as adaptor or scaffolding proteins, can be gleaned from large-scale protein-interaction maps generated by technologies like yeast two-hybrid [6, 7], protein microarrays [8], and MS analysis of immunoprecipitated protein complexes [9, 10]. In contrast, enzymes contribute to biological processes principally through catalysis. Thus, elucidation of the activities of the many thousands of enzymes encoded by eukaryotic and prokaryotic genomes requires knowledge of their endogenous substrates and products. The functional annotation of enzymes in prokaryotic systems has been facilitated by the clever analysis of gene clusters or operons [11, 12], which correspond to sets of genes adjacently located in the genome that encode for enzymes participating in the same metabolic cascade. The assembly of eukaryotic enzymes into metabolic pathways is more problematic, however, as their corresponding genes are not, in general, physically organized into operons, but rather are scattered randomly throughout the genome.

Given the absence of a functional architecture connecting eukaryotic genomes and proteomes, the activities of their enzyme constituents are typically assessed in an empirical manner in vitro by using candidate substrates and purified preparations of protein. The outcome of these "test-tube" biochemistry studies can be difficult to translate into a clear understanding of the roles that enzymes play in living systems, where these proteins are subjected to posttranslational regulation [13] and typically operate as parts of larger metabolic networks [14]. We hypothesized that the determination of endogenous catalytic activities for uncharacterized enzymes could be accomplished directly in living systems by the integrated application of global profiling technologies that survey both the enzymatic proteome and its primary biochemical output (i.e., the metabolome). Here, we have tested this premise by utilizing multidimensional profiling to characterize an integral membrane enzyme of unknown function that is highly elevated in human cancer.

Results

Development of a Selective Inhibitor for the Uncharacterized Enzyme KIAA1363

Previous studies using the chemical proteomic technology activity-based protein profiling (ABPP) [15–17] have identified enzyme activity signatures that distinguish human cancer cells based on their biological properties, including tumor of origin and state of invasiveness [18]. A primary component of these signatures was the protein KIAA1363, an uncharacterized integral membrane hydrolase found to be upregulated in aggressive cancer cells from multiple tissues of origin. Since that time, the mouse ortholog of KIAA1363 has been found to represent a major site of labeling for organophosphorus nerve agents in brain tissue [19]; however, the endogenous metabolic function(s) of this enzyme in mammalian physiology and pathology remains unknown. To investigate the role that KIAA1363 plays in cancer cell metabolism and signaling, a selective inhibitor of this enzyme was generated by competitive ABPP [20, 21].

Key advantages of competitive ABPP include that it can be performed in native proteomes and used to identify inhibitors for enzymes that, like KIAA1363, lack known substrates. Moreover, because inhibitors are screened against many enzymes in parallel, both

*Correspondence: cravatt@scripps.edu
[2]These authors contributed equally to this work.

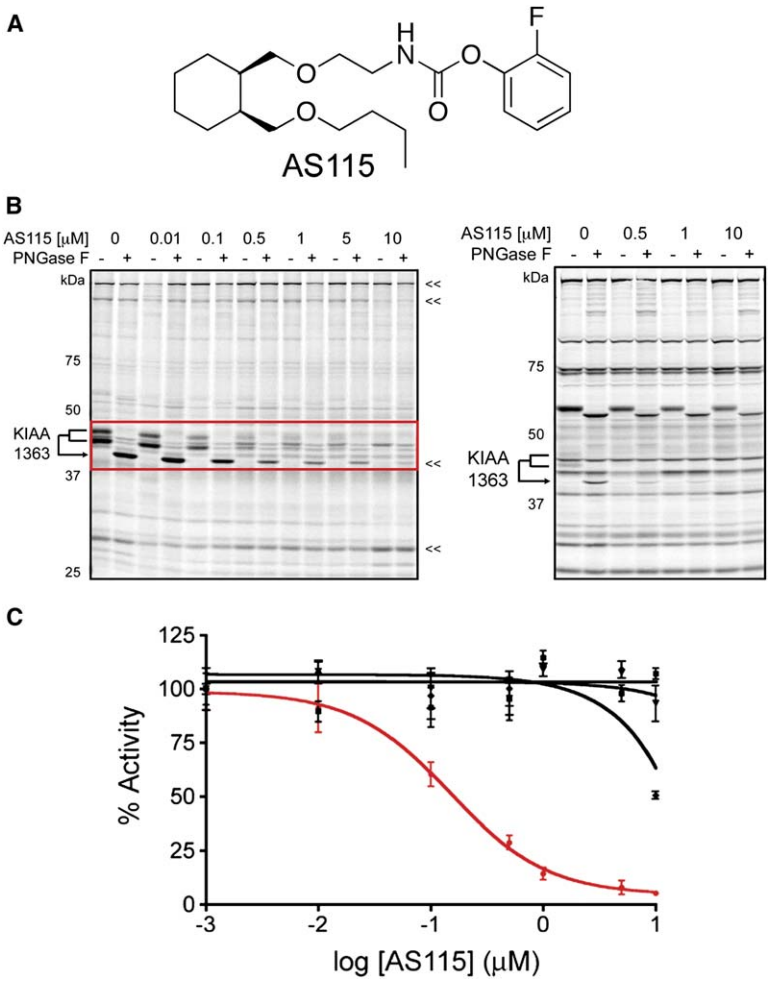

Figure 1. Characterization of AS115, a Selective Inhibitor of the Cancer-Related Enzyme KIAA1363

(A) Structure of AS115.

(B) Effects of AS115 on the membrane (left image) and soluble (right image) serine hydrolase activity profiles of SKOV-3 cells, as judged by competitive ABPP with a rhodamine-tagged FP probe [20]. In-gel fluorescence scanning of FP-labeled proteomes derived from SKOV-3 cells treated in culture with AS115 (0–10 μM) revealed selective inactivation of KIAA1363 (red box). Note that KIAA1363 migrates by SDS-PAGE as a 43 and 45 kDa glycosylated doublet, which, upon treatment with PNGaseF, is converted into a single 40 kDa protein. This protein is predominantly found in the membrane fraction of cancer cells (left image).

(C) AS115 inhibited the FP labeling of KIAA1363 with an IC_{50} value of 150 nM (110–200 nM, 95% confidence limits; red curve), while other serine hydrolases were not affected by this reagent (IC_{50} values > 10 μM, representative hydrolases shown in black curves corresponding to the double-arrowed proteins in [B]). Results represent the average values ± standard error (SE) for three independent experiments.

potency and selectivity factors are simultaneously assigned. Previous competitive ABPP screens with a library of candidate inhibitors and a fluorophosphonate (FP) activity-based probe that targets the serine hydrolase superfamily identified a set of trifluoromethyl ketone (TFMK) inhibitors that showed activity against the mouse ortholog of KIAA1363 in brain extracts [20]. These TFMK inhibitors also inhibited human KIAA1363 in vitro, but they showed only limited activity in living cells (data not shown). We postulated that the in situ activity of KIAA1363 inhibitors could be enhanced by replacing the reversibly binding TFMK group with a carbamate, which inactivates serine hydrolases via a covalent mechanism (Figure S1; see the Supplemental Data available with this article online). Carbamate AS115 (Figure 1A) was synthesized and tested for its effects on the invasive ovarian cancer cell line SKOV-3 by competitive ABPP (Figure 1B). AS115 was found to potently and selectively inactivate KIAA1363, displaying an IC_{50} value of 150 nM, while other serine hydrolase activities were not affected by this agent (IC_{50} values > 10 μM) (Figures 1B and 1C). AS115 also selectively inhibited KIAA1363 in other aggressive cancer cell lines that possess high levels of this enzyme, including the melanoma lines C8161 and MUM-2B (Figure S2B).

Profiling the Metabolic Effects of KIAA1363 Inactivation in Cancer Cells

We next compared the global metabolite profiles of SKOV-3 cells treated with AS115 or vehicle (DMSO) to identify endogenous small molecules regulated by KIAA1363. These experiments were performed by using a recently described, untargeted liquid chromatography-mass spectrometry (LC-MS) platform for comparative metabolomics [22]. AS115 (10 μM, 4 hr) was found to cause a dramatic reduction in the levels of a specific set of lipophilic metabolites (*m/z* 317, 343, and 345) in SKOV-3 cells (Figure 2A). These KIAA1363-regulated metabolites did not correspond to any of the typical lipid species found in cells, including free fatty acids, phospholipids, ceramides, and monoacylglycerides, none of which were significantly altered by AS115 treatment (Table S1). High-resolution MS of the *m/z* 317 metabolite provided a molecular formula of $C_{19}H_{40}O_3$ (Figure 2B), which suggests that this compound might represent a monoalkylglycerol ether bearing a C16:0 alkyl chain (C16:0 MAGE). This structure assignment was corroborated by tandem MS and LC analysis, in which the endogenous *m/z* 317 product and synthetic C16:0 MAGE displayed equivalent fragmentation and migration patterns, respectively (Figure S3). By extension, the *m/z* 343 and 345 metabolites were interpreted to represent

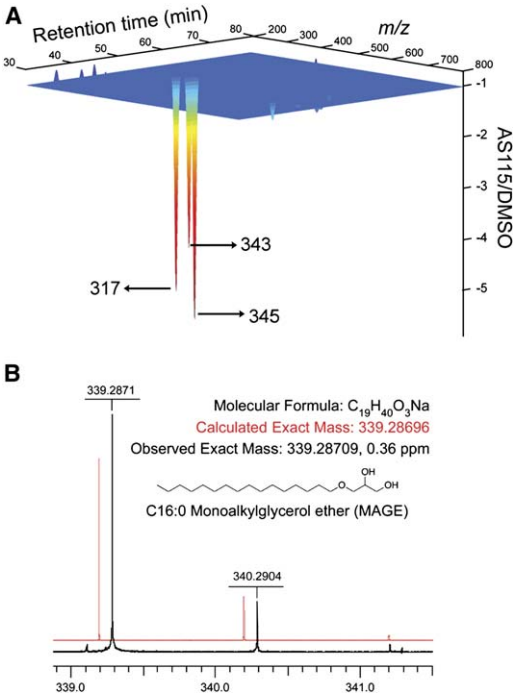

Figure 2. Pharmacological Inhibition of KIAA1363 Reduces Monoalkylglycerol Ether, MAGE, Levels in Human Cancer Cells

(A) Global metabolite profiling of AS115-treated SKOV-3 cells (10 μM AS115, 4 hr) with untargeted LC-MS methods [22] revealed a specific reduction in a set of structurally related metabolites with *m/z* values of 317, 343, and 345 ($p < 0.001$ for AS115- versus DMSO-treated SKOV-3 cells). Results represent the average fold change for three independent experiments. See Table S1 for a more complete list of metabolite levels.

(B) High-resolution MS analysis of the sodium adduct of the purified *m/z* 317 metabolite provided a molecular formula of $C_{19}H_{40}O_3$, which, in combination with tandem MS and LC analysis (Figure S3), led to the determination of the structure of this small molecule as C16:0 monoalkylglycerol ether (C16:0 MAGE).

the C18:1 and C18:0 MAGEs, respectively. Targeted LC-MS analysis with a ^{13}C-MAGE internal standard provided estimates of the absolute levels of MAGEs in SKOV-3 cells, revealing that the C16:0 species was the most abundant member of this lipid family (Table S2). MAGE lipids were also significantly reduced in C8161 and MUM-2B melanoma cells after treatment with AS115 (Figure S4). In contrast, a control carbamate inhibitor, URB597, which targets other hydrolytic enzymes [23], but not KIAA1363, did not affect MAGE levels in cancer cells (Figure S4).

Biochemical Characterization of KIAA1363 as a 2-Acetyl MAGE Hydrolase

The correlation between KIAA1363 inactivation and reduced MAGE levels suggests that these lipids are products of a KIAA1363-catalyzed reaction. A primary route for the biosynthesis of MAGEs has been proposed to occur via the enzymatic hydrolysis of their 2-acetyl precursors [24, 25]. This 2-acetyl MAGE hydrolysis activity was first detected in cancer cell extracts over a decade ago [25], but, to date, it has eluded molecular characterization. To test whether KIAA1363 functions as a 2-acetyl MAGE hydrolase, this enzyme was transiently transfected into COS7 cells. KIAA1363-transfected cells possessed significantly higher 2-acetyl MAGE hydrolase activity compared to mock-transfected cells, and this elevated activity was blocked by treatment with AS115 (Figure 3A). In contrast, KIAA1363- and mock-transfected cells showed no differences in their respective hydrolytic activity for 2-oleoyl MAGE, monoacylglycerols, or phospholipids (e.g., platelet-activating factor [PAF], phosphatidylcholine) (Figure S5A). These data indicate that KIAA1363 selectively catalyzes the hydrolysis of 2-acetyl MAGEs to MAGEs.

Further biochemical studies indicated that KIAA1363 is the principal 2-acetyl MAGE hydrolase in cancer cells. First, 2-acetyl MAGE hydrolase activity, like that of KIAA1363, was predominantly associated with SKOV-3 membranes (Figure S5B). Additionally, fractionation of the SKOV-3 membrane proteome by Q chromatography revealed a tight relationship between KIAA1363 levels and 2-acetyl MAGE hydrolase activity (Figure S5C). Third, SKOV-3 cells possessed much greater 2-acetyl MAGE hydrolase activity compared to the noninvasive ovarian cancer line OVCAR-3 (Figure 3B), correlating well with their respective levels of KIAA1363 (Figure 3C).

KIAA1363 Regulates an Ether Lipid Signaling Network that Bridges Platelet-Activating Factor and the Lysophospholipids

Examination of the Kyoto Encyclopedia of Genes and Genomes (KEGG) database [26] suggests that the KIAA1363-MAGE pathway might serve as a unique metabolic node linking the PAF [27] and lysophospholipid [28] signaling systems in cancer cells (Figure 4A). To test this premise, the major components of this small-molecule network were measured by targeted LC-MS analysis in AS115- and vehicle-treated SKOV-3 cells. AS115 was found to reduce the levels of not only MAGEs, but also alkyl-LPC and alkyl-LPA (Figure 4B). Consistent with a direct pathway leading from MAGEs to these lysophospholipids, addition of ^{13}C-MAGE to SKOV-3 cells resulted in the formation of ^{13}C-labeled alkyl-LPC and alkyl-LPA (Figure 4C). Conversely, the levels of 2-acetyl MAGE in SKOV-3 cells, as judged by metabolic labeling experiments, were significantly stabilized by treatment with AS115, which, in turn, led to an accumulation of PAF (Figure 4D). Basal levels of 2-acetyl MAGE and PAF were not significantly altered by AS115, which may be related to the relatively short duration of action of this inhibitor or to the regulation of endogenous levels of these lipids by alternative rate-limiting enzymatic pathways. Finally, a comparison of the metabolite profiles of SKOV-3 and OVCAR-3 cells revealed significantly higher levels of MAGE, alkyl-LPC, and alkyl-LPA in the former line (Figure 4E). These data indicate that the lysophospholipid branch of the MAGE network is elevated in aggressive cancer cells, and that this metabolic shift is regulated by KIAA1363.

Stable Knockdown of KIAA1363 Impairs Tumor Growth In Vivo

We next asked whether KIAA1363 contributes to cancer pathogenesis in vivo. This question could not be directly addressed by using the KIAA1363 inhibitor AS115 because this agent lacked the pharmacokinetic properties suitable for long-term treatments in vivo (data not

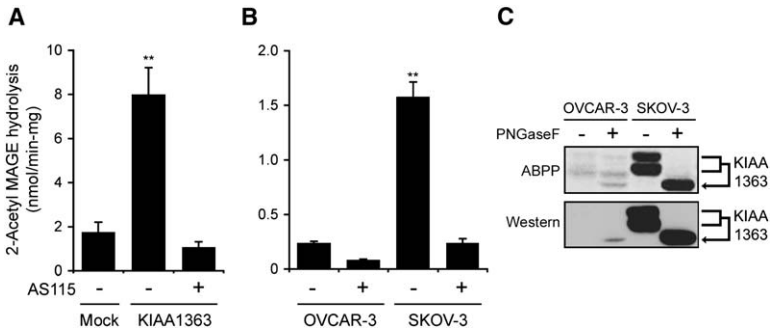

Figure 3. KIAA1363 Is a 2-Acetyl MAGE Hydrolase

(A) COS7 cells transiently transfected with a KIAA1363 cDNA in the pcDNA3 expression vector showed significantly greater 2-acetyl MAGE hydrolase activity compared to mock-transfected cells (transfected with empty pcDNA3 vector). Pretreatment with AS115 (10 μM) blocked the hydrolytic activity of KIAA1363-transfected cells. **, $p < 0.01$ for KIAA1363-transfected cells versus mock-transfected or AS115-treated cells.

(B and C) (B) The invasive ovarian cancer line SKOV-3 possessed significantly higher 2-acetyl MAGE hydrolase activity compared to the noninvasive ovarian cancer line OVCAR-3, which correlated well with the respective levels of KIAA1363 in these cells, as judged by ABPP ([C], upper panel) or western blotting with anti-KIAA1363 antibodies ([C], lower panel). **, $p < 0.01$ for SKOV-3 cells versus OVCAR-3 cells or AS115-treated cells. Results represent the average values ± SE for 3–6 independent experiments.

shown). Therefore, we generated a SKOV-3 line in which the expression of KIAA1363 was selectively and stably decreased by a short-hairpin RNA (shRNA)-mediated interference vector (shKIAA1363 cells). An additional control line (shControl) in which a distinct hydrolytic enzyme (dipeptidylpeptidase IV [DPPIV]) was knocked down by a specific shRNA probe was also generated. shKIAA1363 cells showed an ~75% reduction of this enzyme compared to control cells (shControl or parental SKOV-3 cells) (Figure 5A), which correlated with a similar magnitude decrease in 2-acetyl MAGE hydrolase activity (Figure 5B) and the levels of MAGE, alkyl-LPC, and alkyl-LPA lipids (Figure 5C). The levels of other hydrolytic enzymes were not affected in shKIAA1363 cells, as judged by gel-based ABPP (Figure S6).

shKIAA1363 and control SKOV-3 cells were next compared for their tumor growth capacity by subcutaneous injection into immune-deficient mice. shKIAA1363 SKOV-3 cells exhibited significantly reduced tumor growth rates compared to either shControl cells or the parental SKOV-3 line (Figure 6A). shRNA-mediated knockdown of KIAA1363 was also performed in the aggressive breast cancer line MDA-MB-231, resulting in lowered MAGE and lysophosopholipid levels in these cells and impaired tumor growth in vivo (Figure S7).

The decrease in tumorigenic potential of shKIAA1363 cells was not associated with a change in proliferation potential in vitro (Figure S8). shKIAA1363 cells were, however, impaired in their in vitro migration capacity compared to control cells (Figure 6B). To discern whether any of the lipids regulated by KIAA1363 might contribute to cancer cell migration, we tested the pharmacological effects of these compounds on shKIAA1363 cells. Neither MAGE nor alkyl-LPC impacted cancer cell migration at concentrations up to 1 μM (Figure 6B). In contrast, alkyl-LPA (10 nM) completely rescued the reduced migratory activity of shKIAA1363 cells. Collectively, these results indicate that KIAA1363 contributes to the pathogenic properties of cancer cells in vitro and in vivo, possibly through regulating the levels of the bioactive lipid LPA.

Discussion

We have determined by integrated enzyme and small-molecule profiling that KIAA1363, a protein of previously unknown function, is a 2-acetyl MAGE hydrolase that serves as a key regulator of a lipid signaling network that contributes to cancer pathogenesis. Although we cannot yet conclude which of the specific metabolites regulated by KIAA1363 supports tumor growth in vivo, the rescue of the reduced migratory phenotype of shKIAA1363 cancer cells by LPA is consistent with previous reports showing that this lipid signals through a family of G protein-coupled receptors to promote cancer cell migration and invasion [28–30]. LPA is also an established biomarker in ovarian cancer, and the levels of this metabolite are elevated nearly 10-fold in ascites fluid and plasma of patients with ovarian cancer [31]. Our results suggest that additional components in the KIAA1363-ether lipid network, including MAGE, alkyl LPC, and KIAA1363 itself, might also merit consideration as potential diagnostic markers for ovarian cancer. Consistent with this premise, our preliminary analyses have revealed highly elevated levels of KIAA1363 in primary human ovarian tumors compared to normal ovarian tissues (data not shown). The heightened expression of KIAA1363 in several other cancers, including breast [18, 32], melanoma [18], and pancreatic cancer [33], indicates that alterations in the KIAA1363-ether lipid network may be a conserved feature of tumorigenesis. Considering further that reductions in KIAA1363 activity were found to impair tumor growth of both ovarian and breast cancer cells, it is possible that inhibitors of this enzyme may prove to be of value for the treatment of multiple types of cancer.

Looking forward, it is worth discussing the potential generality of the multidimensional profiling strategy put forth in this study for the functional annotation of other uncharacterized enzymes in eukaryotic and prokaryotic proteomes. The development of a selective inhibitor to perturb KIAA1363 function was predicated on the availability of an activity-based proteomics probe for this enzyme. Such probes are now available for many enzyme classes that participate in cell metabolism, including all major families of hydrolases [15], [34–39], glycosidases [40, 41], kinases [42, 43], glutathione *S*-transferases [44, 45], and oxidoreductases [45, 46], suggesting that a large swath of the enzyme proteome could be addressed by following the experimental strategy presented herein. For enzymes that lack cognate activity-based probes, RNA interference (RNAi) methods, coupled with metabolic profiling, may suffice for their functional annotation. Indeed, if one takes KIAA1363

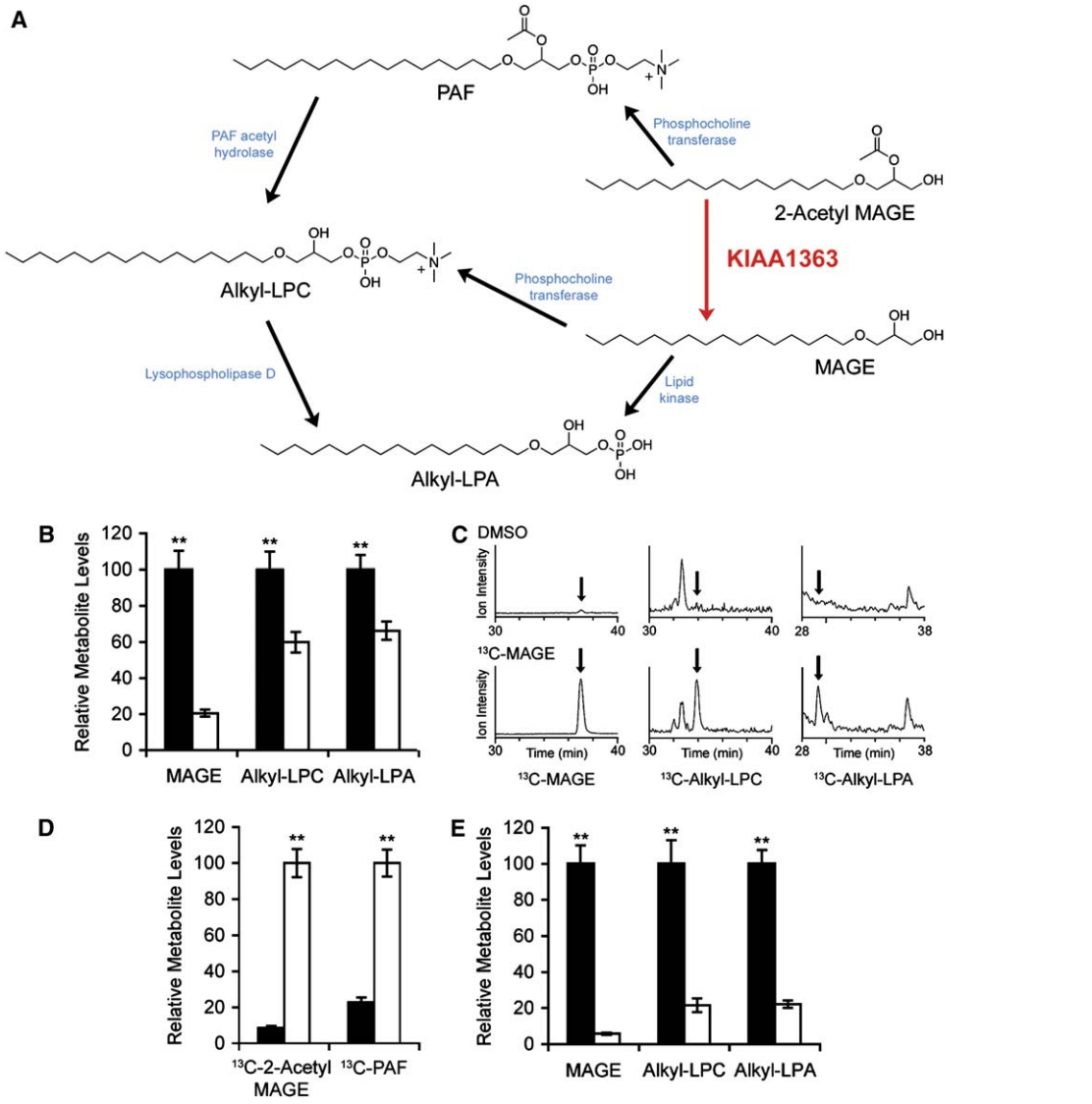

Figure 4. KIAA1363 Serves as a Key Enzymatic Node in a Metabolic Network that Connects the PAF and Lysophospholipid Families of Signaling Lipids

(A) Network diagram showing metabolite and enzyme components (metabolites are shown with a C16:0 alkyl chain for clarity of presentation).

(B) Treatment of SKOV-3 cells with AS115 (10 μM, 4 hr) reduced multiple components of the metabolite network, including MAGE, alkyl-LPC, and alkyl-LPA. **, $p < 0.01$ for AS115- (white bars) versus DMSO- (black bars) treated SKOV-3 cells.

(C) Metabolic labeling of SKOV-3 cells with ^{13}C-MAGE (10 μM, 4 hr) shows that this lipid can be directly converted to LPC and LPA. Data are normalized to show relative MS signals for each lipid and its ^{13}C variant. No accumulation of ^{13}C-2-acetyl MAGE or ^{13}C-PAF was observed after treatment with ^{13}C-MAGE.

(D) SKOV-3 cells treated with AS115 (white bar; 10 μM AS115, 0.5 hr) exhibited significantly reduced degradation of ^{13}C-2-acetyl MAGE (10 μM, 1 hr) compared to DMSO-treated control cells (black bar). Accumulation of ^{13}C-PAF was also observed in AS115-treated cells. **, $p < 0.01$ for AS115- versus DMSO-treated SKOV-3 cells.

(E) MAGE and lysophospholipids (LPC and LPA) are highly elevated in SKOV-3 cells (black bars) compared to OVCAR-3 cells (white bars). **, $p < 0.01$ for SKOV-3 versus OVCAR-3 cells. Results represent the average values ± SE for 3–6 independent experiments.

as a case study, the metabolic effects of perturbing this enzyme by a small-molecule inhibitor or RNAi proved complementary. The former approach allowed for visualization of the acute effects of KIAA1363 inactivation, facilitating the discovery of direct products (MAGEs) of this enzyme. The constitutive disruption of KIAA1363 function by RNAi produced more dramatic network-wide changes that impacted not only the direct, but also downstream, metabolites (e.g., lysophospholipids) regulated by this enzyme. These findings suggest that sole reliance on RNAi should enable the discovery of direct products of enzymes in living systems, although the identification of these molecules may require follow-up biochemical assays to distinguish them from secondary metabolites in enzyme-regulated networks.

Independent of the experimental strategy employed for enzyme inactivation, a primary advantage of metabolite profiling in native biological systems is that it

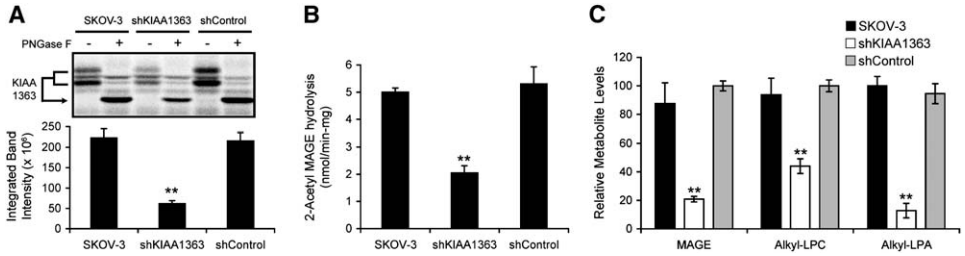

Figure 5. Metabolic Effects of Stable shRNA-Mediated Knockdown of KIAA1363 in Human Cancer Cells

(A) SKOV-3 cells possessing a stably integrated shRNA specific for KIAA1363 showed an ~75% reduction of this enzyme activity compared to parental SKOV-3 cells or cells possessing a control shRNA that targeted the unrelated serine hydrolase DPPIV (shControl), as judged by ABPP. The levels of other serine hydrolases were not affected in shKIAA1363 cells (Figure S6).

(B and C) shKIAA1363 SKOV-3 cells displayed significant reductions in (B) 2-acetyl MAGE hydrolase activity and (C) MAGE, alkyl-LPC, and alkyl-LPA levels compared to control cells. ** $p < 0.01$, for shKIAA1363 (white bars) versus control cells (parental SKOV-3 [black] or shControl [gray]). Results represent the average values ± SE for six independent experiments.

circumvents some of the most laborious and time-consuming steps that accompany the in vitro analysis of enzymes (i.e., recombinant expression and purification, candidate substrate screening), and, at the same time, generates data sets that are more directly related to their endogenous activities. Expanded systems biology efforts to assemble the full complement of enzymes encoded by the human genome into metabolic and signaling networks that contribute to complex pathologies, like cancer, should lead to the discovery of many new markers and targets for disease diagnosis and treatment.

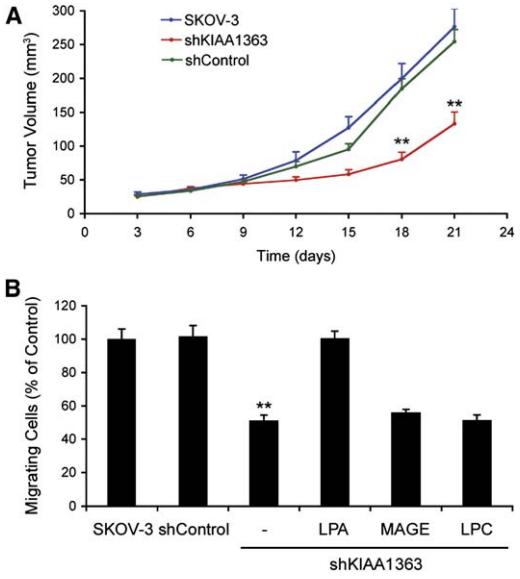

Figure 6. KIAA1363 Contributes to Ovarian Tumor Growth and Cancer Cell Migration

(A) shKIAA1363 SKOV-3 cells showed significantly impaired tumor growth rates in immune-deficient mice compared to control cells. **, $p < 0.01$ for shKIAA1363 versus control cells. n = 7–10 mice per group.

(B) shKIAA1363 SKOV-3 cells show reduced migration in vitro compared to control cells. The reduced migration of shKIAA1363 cells is reversed by treatment with C16:0-alkyl-LPA (10 nM), but not C16:0-MAGE or C16:0-alkyl LPC (each tested from 10 nM to 1 μM; data shown for 100 nM). ** $p < 0.01$, for shKIAA1363 versus control cells or shKIAA1363 cells treated with LPA. Results represent the average values ± SE for 3–4 independent experiments.

Significance

The complete genome sequences of several eukaryotic and prokaryotic organisms have revealed a daunting number of uncharacterized proteins in need of functional annotation. For enzymes, in particular, the elucidation of endogenous substrates and products is imperative for integrating these proteins into the biochemical networks that govern health and disease. Here, we present a multidimensional systems biology strategy that addresses this problem. By combining activity-based proteomic and metabolomic methods, we have determined that the uncharacterized integral membrane enzyme KIAA1363, which is highly elevated in human cancer, serves as a critical node in an ether lipid signaling network that links platelet-activating factor and the lysophospholipids. Disruption of this small-molecule network through the impairment of KIAA1363 activity reduced cancer cell migration and tumor growth in vivo, promoting this enzyme as a potential therapeutic target for the treatment of cancer. More generally, these results showcase the value of integrated molecular profiling as an experimental strategy to annotate uncharacterized enzymes directly in living systems.

Experimental Procedures

Materials

C17:0 lysophosphatidic acid (LPA), C16:0 2-acetyl MAGE, PAF, and phosphtidylcholine were purchased from Avanti Lipids. C15:0 monoacylglycerol (MAG) was purchased from Larodan (Sweden). FP-rhodamine was synthesized by following previously described procedures [47, 48]. Synthesis of ^{13}C-C16:0 MAGE was carried out as described previously [49], and targeted acetylation to generate ^{13}C-C16:0 2-acetyl MAGE was performed as reported [50]. The synthesis of AS115 is detailed in Supplemental Data.

Plasmids

Human KIAA1363 construct was generated by PCR with primers 5′-CGCGGATCCATGAGGTCGTCCTGTGTCCTG-3′ and 5′-CGGAATTCTTACAGGTTTTGATCTAGCC-3′. PCR products were subcloned into the pcDNA3.1+ vector (Invitrogen) by using BamHI and EcoRI restriction sites.

In Situ Inhibition of KIAA1363 in Cancer Cells

The human ovarian cancer cell line were obtained form the National Cancer Institute's Developmental Therapeutics Program. The melanoma lines C8161 and MUM-2B were obtained from Mary Hendrix.

Cells were maintained in RPMI medium 1640 with 10% (v/v) fetal calf serum at 37°C in a humidified atmosphere of 5% CO_2/95% air. At ~80% confluency, cells were trypsinized and counted with the aid of a hemocytometer, and 2.5×10^6 cells were plated in 6 cm dishes. A total of 20 hr after plating, cells were washed twice with PBS and supplemented with serum-free RPMI containing 0.5% BSA (Sigma) (BSA-RPMI) with AS115 (0.01–10 μM) or vehicle (DMSO) at 0.1%. After incubation for 4 hr, the cells were harvested and analyzed by ABPP or LC-MS.

ABPP Analysis of Cancer Cell Proteomes

Cells were washed twice and scraped in ice-cold PBS. Cell pellets were isolated by centrifugation at 1,400 × g for 3 min and dounce-homogenized in Tris buffer (50 mM Tris-HCl [pH 8.0]). Membrane proteomes were isolated by centrifugation at 4°C at 100,000 × g to provide a soluble fraction and a particulate fraction (pellet). The pellet was washed and resuspended in Tris buffer by sonication to provide a membrane fraction. Proteomes protein concentrations were determined by a protein assay kit (Bio-Rad), adjusted to a final concentration of 1 mg/ml in Tris buffer, and treated with 2 μM FP-rhodamine for 30 min at room temperature (50 μl total reaction volume). After labeling, a portion of each sample was treated with PNGaseF (New England Biolabs) to provide deglycosylated proteomes. Reactions were quenched with one volume of standard 2× SDS/PAGE loading buffer (reducing), separated by SDS/PAGE (10% acrylamide), and visualized in-gel with a Hitachi FMBio IIe flatbed fluorescence scanner (MiraiBio). Integrated band intensities were calculated for the labeled proteins and averaged from three independent cell samples to determine the level of each enzyme activity. IC_{50} values were determined from dose-response curves from three trials at each inhibitor concentration by using Prism software (GraphPad) to obtain values with 95% confidence intervals.

Analysis of Cancer Cell Metabolomes

Cell pellets were harvested by scraping, isolated by centrifugation at 1,400 × g, and dounce-homogenized in 4 ml of a 2:1:1 mixture of chloroform:methanol:Tris buffer. Samples that were analyzed by targeted LC-MS were homogenized in the presence of the following synthetic standards: C15:0 MAG (50 pmol), C17:0 LPA (50 pmol), and ^{13}C-C16:0 MAGE (25 pmol). Organic and aqueous layers were separated by centrifugation at 1,260 × g for 5 min. The organic layer was then removed, dried under a stream of N_2, and resolubilized in 100 μl chloroform, of which 30 μl was analyzed by LC-MS. Extraction of LPA was performed by acidifying the remaining aqueous layer to a final concentration of 5% formic acid, followed by the addition of 2 ml chloroform. The mixture was vortexed, and the organic layer was removed, concentrated to dryness, and dissolved in 100 μl chloroform, of which 30 μl was analyzed by LC-MS.

LC-MS analysis was performed by using an Agilent 1100 LC-MSD SL instrument. LC separation was achieved with a Gemini reverse-phase C18 column (5 μm, 4.6 mm × 50 mm) from Phenomonex together with a precolumn (C18, 3.5 μm, 2 mm × 20 mm). Mobile phase A was composed of a 95:5 ratio of water:methanol, and mobile phase B consisted of 2-propanol, methanol, and water in a 60:35:5 ratio. Solvent modifiers such as 0.1% formic acid and 0.1% ammonium hydroxide were used to assist ion formation as well as to improve the LC resolution in both positive and negative ionization modes, respectively. The flow rate for each run started at 0.1 ml/min for 5 min, to alleviate backpressure associated with injecting chloroform. The gradient started at 0% B and increased linearly to 100% B over the course of 40 min with a flow rate of 0.4 ml/min, followed by an isocratic gradient of 100% B for 7 min before equilibrating for 8 min at 0% B with a flow rate of 0.5 ml/min. MS analysis was performed with an electrospray ionization (ESI) source. The capillary voltage was set to 3.0 kV, and the fragmentor voltage was set to 100 V. The drying gas temperature was 350°C, the drying gas flow rate was 10 L/min, and the nebulizer pressure was 35 psi. Untargeted data were collected by using a mass range of 200–1000 Da and were exported as common data format (.CDF) files for computational analysis. Differentially expressed metabolites between sample pairs were identified by using the XCMS analyte profiling software (http://metlin/download), which aligns and quantifies the relative signal intensities of mass peaks from multiple LC-MS traces [51]. Significant inhibitor-sensitive peak changes were confirmed by manual quantification by using the area under the peak normalized to total ion current. Targeted LC-MS measurements were made by using selected ion monitoring (SIM). Peaks were quantified by measuring the area under the peak and were normalized to an internal standard (C15:0 MAG) of endogenous lipid (palmitic acid). Absolute MAGE levels were estimated by comparison to a ^{13}C-MAGE standard.

Preparative HPLC Purification of C16:0 MAGE

Large-scale preparations of cultured SKOV-3 cells (~4×10^7 cells) were plated in 10 × 15 cm dishes and incubated in serum-free media for 48 hr. Cells pellets were isolated as described above and homogenized in 8 ml of a 2:1:1 mixture of chloroform:methanol:Tris buffer. The organic layer was removed, dried under a stream of N_2, and resolubilzed in 200 μl chloroform. The metabolite extracts were LC purified by using a Hitachi L-7150 HPLC system equipped with a semipreparative C18 reverse-phase column (5 μm, 10 mm × 50 mm) from Phenomonex. Mobile phase A was composed of a 95:5 ratio of water:methanol, with 0.1% formic acid, and mobile phase B consisted of 2-propanol, methanol, and water in a 60:35:5 ratio, with 0.1% formic acid. The gradient started at 0% B and then increased linearly to 100% B over the course of 60 min, followed by an isocratic gradient of 100% B for 20 min at a flow rate of 2.5 ml/min. Fractions, one per minute, were collected by using a Gilson FC 203B fraction collector. Fractions containing the 317 metabolite were identified by MS analysis, collected, extracted with chloroform, and concentrated to dryness, and the residue was then dissolved in a minimal amount of solvent B (200–300 μl) for exact mass analysis.

Metabolic Labeling of Cells with ^{13}C-2-Acetyl MAGE and ^{13}C-MAGE

Cells were cultured and maintained as described above. Cells used for ^{13}C-2-acetyl MAGE experiments were incubated in BSA-RPMI containing inhibitor or vehicle for 30 min. BSA-RPMI medium was then removed, supplemented with 10 μM ^{13}C-2-acetyl MAGE or DMSO, and reapplied to cells. After incubation for 1 hr, the cells were harvested and metabolomes were analyzed by LC-MS. ^{13}C-MAGE experiments were conducted by addition of ^{13}C-MAGE or DMSO containing BSA-RPMI directly after washing with PBS. Cells were then incubated for 4 hr, harvested, and analyzed by LC-MS.

Fourier Transform Mass Spectrometry, FTMS, Experiments

High-accuracy measurements were performed in the positive ion mode by using a Bruker (Billerica, MA) APEX III (4.7 T) FTMS instrument equipped with an Apollo electrospray source. The collected LC fractions were mixed with a collection of small-molecule standards and directly infused at 3 μl/min by using a Harvard Apparatus (Holliston, MA) syringe pump. Pneumatic assist at a backing pressure of 60 psi was used along with an optimized flow rate of heated counter-current drying gas (300°C). Ion accumulation was performed by using SideKick without pulsed gas trapping. Data acquisition times of approximately 1 min were used, yielding a resolving power of ~13,0000 at *m/z* 446 in broadband in the *m/z* range of 200–2,200. Calculated molecular masses for ions generated by a mixture of small-molecule standards were used to internally calibrated the data.

Sulfonation of C16:0 MAGE

Endogenous HPLC-purified C16:0 MAGE or synthetic standard (Sigma) and 1% (w/v) sulfur trioxide in 4:1 dimethylformamide and pyridine were added to a 4 ml vial with a magnetic stir bar. This mixture was stirred at 70°C for 2 hr. The reaction mixture was then concentrated to dryness under a stream of nitrogen, followed by 1 hr under vacuum, and the residue was then dissolved in a minimal amount of methanol for MS/MS analysis.

Tandem MS Experiments

MS/MS experiments were performed in the negative ion mode by using a Micromass QTof-*Micro*(Manchester, UK) instrument equipped with a Z-spray electrospray source and a lockmass sprayer. The source temperature was set to 110°C with a cone gas flow of 150 l/hr, a desolvation gas temperature of 365°C, and a nebulization gas flow rate of 350 l/hr. The capillary voltage was set a 3.2 kV, and the cone voltage was set at 30 V. The collision energy was set

at 15–35 V. Samples were directly infused at 4 μl/min by using a Harvard Apparatus syringe pump. MS/MS data were collected in the centroid mode over a scan range of *m/z* 70–450 for acquisition times of 2 min.

Enzyme Activity Assays with Lipid Substrates

Membrane and soluble proteomes were adjusted to 0.25 mg/ml in Tris buffer and preincubated with AS115 (10 μM) or DMSO for 15 min. Lipid substrates (2-acetyl MAGE, 2-oleoyl MAGE, phosphatidylcholine, PAF) were assayed at 100 μM in 100 μl proteome at room temperature for various amounts of time (5–40 min), after which reactions were quenched with 200 μl chloroform and 50 μl methanol. Lipid substrates and products were extracted into the organic layer, concentrated to dryness, and resolubilized in 300 μl chloroform prior to LC-MS analysis. MS settings, columns, and mobile phases were similar to those described above. Hydrolysis products were quantified by measuring the area under the peak in comparison to standard curves generated with purified products. Specific activity was determined during the linear phase of enzymatic reactions (i.e., less than 20% product observed). Monoacylglycerol hydrolysis was measured by using a ^{14}C-labeled 2-oleoylglycerol substrate after the conversion to ^{14}C-oleic acid by using a thin-layer chromatography assay. For enzyme assays performed with recombinant KIAA1363, COS7 cells were transiently transfected with the human KIAA1363 cDNA in the mammalian expression vector pcDNA3 by following previously described methods [20].

Q Chromatography Enrichment of KIAA1363

Cell membranes were isolated as described above and solubilized by rotating for 1 hr at 4°C in Tris buffer containing 1% Triton X-100. Detergent-insoluble proteins were removed by centrifugation at 100,000 × g for 45 min. Triton-solubilized proteomes were adjusted to a final protein concentration of 1 mg/ml and subjected to anion-exchange chromatography in Tris buffer with 0.1% Triton X-100 on a Q Sepharose HP column (Amersham Pharmacia Biotech) with a 10 min linear gradient of 0–1 M NaCl at a flow rate of 0.5 ml/min. Fractions were pooled, tested for 2-acetyl MAGE hydrolytic activity, and analyzed by FP-rhodamine as described above.

Western Blotting with Anti-KIAA1363 Polyclonal Antibodies

A KIAA1363-GST fusion protein was generated by subcloning human KIAA1363 into the pGEX4T-3 fusion vector (Amersham Pharmacia Biotech) by using BamHI and EcoRI restriction sites. Rabbit polyclonal antibodies were raised against KIAA1363-GST fusion protein, expressed in *E. coli* BL21 strain according to manufacturer's recommendations (Amersham Pharmacia Biotech), and administered in conjunction with RIBI adjuvant (Corixa). Affinity purification of the anti-KIAA1363 antibodies was conducted by first depleting rabbit antiserum of GST-crossreactive antibodies, followed by isolation of KIAA1363-GST reactive antibodies form the remaining serum as previously described [52].

Preparation of a Xenograft Tumor-Derived SKOV-3 Line

In vivo-derived SKOV-3 lines were established by following previously described procedures [53]. Briefly, a well-established SKOV-3 xenograft tumor growing in the mouse flank was removed aseptically and minced with a razor blade; tumor pieces were transferred into tissue culture flasks with complete medium. After 4 days of culture, when abundant adherent tumor cells were visible, floating tumor debris was removed. Attached cells were then expanded to constitute a propagatable cell population.

RNA Interference Studies in Human Cancer Cell Lines

RNA interference studies were conducted by using a variant of the SKOV-3 line isolated by in vivo passaging in immune-deficient mice. This in vivo-derived SKOV-3 line showed enhanced tumor-forming capacity in vivo compared to the parental line, as has been reported previously [54]. Short-hairpin RNA constructs were subcloned into the pLP-RetroQ acceptor system, and retrovirus was generated by using the AmphoPack-293 Cell Line (Clontech). Hairpin oligonucleotides utilized were: for KIAA1363, 5′-TGTGAACACCCC AATCCTG-3′; for DPPIV, 5′-GATTCTTCTGGGACTGCTG-3′. A pLP-RetroQ vector was developed for tPa by using a validated oligonucleotide sequence purchased from Clontech. Virus containing supernatant from 24–72 hr was collected, concentrated by ultracentrifugation, and, in the presence of 10 μg/ml polybrene, used to stably infect SKOV-3 cells for 48 hr. Infection was followed by 3 days of selection in medium containing 1 μg/ml puromycin, as the retroviral vector contained this selection marker. Infected SKOV-3 cells were expanded and tested for the loss of enzyme activity by ABPP.

Tumor Xenograft Studies

Human cancer xenografts were established by transplanting cancer cell lines ectopically into the flank (SKOV-3) or mammary fat pad (231mfp) of C.B17 SCID mice (Taconic Farms). Briefly, cells were washed two times with PBS, trypsinized, and resuspended in medium containing serum. Next, the harvested cells were washed two times with serum-free medium and resuspended at a concentration of 4.4 × 10^4 cells/μl (or 1.0 × 10^4 cells/μl for 231mfp cells), and 100 μl was injected. Growth of the tumors was measured every 3 days with calipers.

Cell Migration Assay

Migration assays were performed in Transwell chambers with 8 μM pore-sized membranes coated with 10 μg/ml collagen overnight at 4°C (Corning). A total of 24 hr before the start of the migration assay, cancer cell lines were plated at a concentration of 2.25 × 10^6 cells per 10 cm dish. At the start of the migration assay, cells were harvested by washing two times with PBS and were then serum starved in medium containing 0.05% BSA for 4 hr. Serum-starved cells were trypsinized, spun at 1400 × g for 3 min, resuspended, and counted. Cells were diluted to a density of 50,000 cells/ml in medium containing 0.05% BSA, and then 250 μl was placed in the upper chamber of the transwells. Either DMSO, C16:0-alkyl-LPA (10 nM), C16:0-alkyl-LPC (10–1000 nM), or MAGE (10–1000 nM) in medium containing 0.05% BSA was added in the lower chamber, and cells were allowed to migrate for 18 hr. The filters were then fixed and stained with Diff-Quik (Dade Behring). Cells that had not migrated through the chamber were removed with a cotton ball. The cells that migrated were counted at a magnification of 40×, and 6 fields were independently counted from each migration chamber.

Cell Proliferation Assay

Cancer cell lines were plated at a concentration of 6.4 ×10^5, 3.2 × 10^5, 1.6 ×10^5, and 8 ×10^4 cells per 10 cm dish in triplicate. They were then counted 2, 4, 6, and 8 days after plating with trypan blue (Sigma).

Supplemental Data

Supplemental Data include a comparison of the relative metabolite levels in KIAA1363-inhibited versus control cancer lines, the absolute level of MAGE lipids in SKOV-3 cells, the competitive ABPP analysis of AS115, the structural analysis of endogenous and synthetic C16:0 MAGE, the levels of MAGE lipids in KIAA1363-inhibited and control cancer lines, the activity of KIAA1363 with a panel of lipid substrates, and the effect of knocking down KIAA1363 levels by shRNA on the activity of other serine hydrolases. These data are available at http://www.chembiol.com/cgi/content/full/13/10/1041/DC1/.

Acknowledgments

We thank S. Trauger, L. Want, G. O'Maille, and G. Siuzdak, for assistance with the MS characterization of purified MAGEs; B. Mueller for assistance with the tumor xenograft models; and members of the Cravatt laboratory for helpful discussion and critical reading of the manuscript. This work was supported by the National Institutes of Health (CA087660), the California Breast Cancer Research Foundation (B.F.C. and K.P.C.), the Achievement Reward for College Scientists Foundation (K.P.C.), a Merck Fellowship from the Life Sciences Research Foundation (A.S.), Burroughs Wellcome Fund Career Award (A.S.), and the Skaggs Institute for Chemical Biology.

Received: August 5, 2006
Accepted: August 22, 2006
Published: October 20, 2006

References

1. Patterson, S.D., and Aebersold, R. (2003). Proteomics: the first decade and beyond. Nat. Genet. *33*, 311–323.
2. Brown, P.O., and Botstein, D. (1999). Exploring the new world of the genome with DNA microarrays. Nat. Genet. *21*, 33–37.
3. Golub, T.R., Slonim, D.K., Tamayo, P., Huard, C., Gaasenbeek, M., Mesirov, J.P., Coller, H., Loh, M.L., Downing, J.R., Caligiuri, M.A., et al. (1999). Molecular classification of cancer: class discovery and class prediction by gene expression. Science *286*, 531–537.
4. Yates, J.R., III. (2004). Mass spectral analysis in proteomics. Annu. Rev. Biophys. Biomol. Struct. *33*, 297–316.
5. Domon, B., and Aebersold, R. (2006). Mass spectrometry and protein analysis. Science *312*, 212–217.
6. Evangelista, C., Lockshon, D., and Fields, S. (1996). The yeast two-hybrid system: prospects for protein linkage maps. Trends Cell Biol. *6*, 196–199.
7. Uetz, P. (2002). Two-hybrid arrays. Curr. Opin. Chem. Biol. *6*, 57–62.
8. Jones, R.B., Gordus, A., Krall, J.A., and MacBeath, G. (2006). A quantitative protein interaction network for the ErbB receptors using protein microarrays. Nature *439*, 168–174.
9. Gavin, A.C., Bosche, M., Krause, R., Grandi, P., Marzioch, M., Bauer, A., Schultz, J., Rick, J.M., Michon, A.M., Cruciat, C.M., et al. (2002). Functional organization of the yeast proteome by systematic analysis of protein complexes. Nature *415*, 141–147.
10. Ho, Y., Gruhler, A., Heilbut, A., Bader, G.D., Moore, L., Adams, S.L., Millar, A., Taylor, P., Bennett, K., Boutilier, K., et al. (2002). Systematic identification of protein complexes in *Saccharomyces cerevisiae* by mass spectrometry. Nature *415*, 180–183.
11. Haller, T., Buckel, T., Retey, J., and Gerlt, J.A. (2000). Discovering new enzymes and metabolic pathways: conversion of succinate to propionate by *Escherichia coli*. Biochemistry *39*, 4622–4629.
12. Vaillancourt, F.H., Yeh, E., Vosburg, D.A., O'Connor, S.E., and Walsh, C.T. (2005). Cryptic chlorination by a non-haem iron enzyme during cyclopropyl amino acid biosynthesis. Nature *436*, 1191–1194.
13. Kobe, B., and Kemp, B.E. (1999). Active site-directed protein regulation. Nature *402*, 373–376.
14. Remy, I., and Michnick, S.W. (2001). Visualization of biochemical networks in living cells. Proc. Natl. Acad. Sci. USA *98*, 7678–7683.
15. Liu, Y., Patricelli, M.P., and Cravatt, B.F. (1999). Activity-based protein profiling: the serine hydrolases. Proc. Natl. Acad. Sci. USA *96*, 14694–14699.
16. Jessani, N., and Cravatt, B.F. (2004). The development and application of methods for activity-based protein profiling. Curr. Opin. Chem. Biol. *8*, 54–59.
17. Berger, A.B., Vitorino, P.M., and Bogyo, M. (2004). Activity-based protein profiling: applications to biomarker discovery, in vivo imaging and drug discovery. Am. J. Pharmacogenomics *4*, 371–381.
18. Jessani, N., Liu, Y., Humphrey, M., and Cravatt, B.F. (2002). Enzyme activity profiles of the secreted and membrane proteome that depict cancer invasiveness. Proc. Natl. Acad. Sci. USA *99*, 10335–10340.
19. Nomura, D.K., Leung, D., Chiang, K.P., Quistad, G.B., Cravatt, B.F., and Casida, J.E. (2005). A brain detoxifying enzyme for organophosphorus nerve poisons. Proc. Natl. Acad. Sci. USA *102*, 6195–6200.
20. Leung, D., Hardouin, C., Boger, D.L., and Cravatt, B.F. (2003). Discovering potent and selective reversible inhibitors of enzymes in complex proteomes. Nat. Biotechnol. *21*, 687–691.
21. Greenbaum, D., Baruch, A., Hayrapetian, L., Darula, Z., Burlingame, A., Medzihradszky, K.F., and Bogyo, M. (2002). Chemical approaches for functionally probing the proteome. Mol. Cell. Proteomics *1*, 60–68.
22. Saghatelian, A., Trauger, S.A., Want, E.J., Hawkins, E.G., Siuzdak, G., and Cravatt, B.F. (2004). Assignment of endogenous substrates to enzymes by global metabolite profiling. Biochemistry *43*, 14332–14339.
23. Kathuria, S., Gaetani, S., Fegley, D., Valino, F., Duranti, A., Tontini, A., Mor, M., Tarzia, G., La Rana, G., Calignano, A., et al. (2003). Modulation of anxiety through blockade of anandamide hydrolysis. Nat. Med. *9*, 76–81.
24. Qian, C.G., Lee, T.C., and Snyder, F. (1989). Metabolism of platelet activating factor (PAF) and related ether lipids by neonatal rat myocytes. J. Lipid Mediat. *1*, 113–123.
25. Blank, M.L., Smith, Z.L., Cress, E.A., and Snyder, F. (1990). Characterization of the enzymatic hydrolysis of acetate from alkylacetylglycerols in the de novo pathway of PAF biosynthesis. Biochim. Biophys. Acta *1042*, 153–158.
26. Kanehisa, M., Goto, S., Kawashima, S., Okuno, Y., and Hattori, M. (2004). The KEGG resource for deciphering the genome. Nucleic Acids Res. *32*, D277–D280.
27. Prescott, S.M., Zimmerman, G.A., Stafforini, D.M., and McIntyre, T.M. (2000). Platelet-activating factor and related lipid mediators. Annu. Rev. Biochem. *69*, 419–445.
28. Mills, G.B., and Moolenaar, W.H. (2003). The emerging role of lysophosphatidic acid in cancer. Nat. Rev. Cancer *3*, 582–591.
29. Xu, Y., Tanaka, M., Arai, H., Aoki, J., and Prestwich, G.D. (2004). Alkyl lysophosphatidic acid and fluoromethylene phosphonate analogs as metabolically-stabilized agonists for LPA receptors. Bioorg. Med. Chem. Lett. *14*, 5323–5328.
30. Jourquin, J., Yang, N., Kam, Y., Guess, C., and Quaranta, V. (2006). Dispersal of epithelial cancer cell colonies by lysophosphatidic acid (LPA). J. Cell. Physiol. *206*, 337–346.
31. Xiao, Y.J., Schwartz, B., Washington, M., Kennedy, A., Webster, K., Belinson, J., and Xu, Y. (2001). Electrospray ionization mass spectrometry analysis of lysophospholipids in human ascitic fluids: comparison of the lysophospholipid contents in malignant vs nonmalignant ascitic fluids. Anal. Biochem. *290*, 302–313.
32. Jessani, N., Young, J.A., Diaz, S.L., Patricelli, M.P., Varki, A., and Cravatt, B.F. (2005). Class assignment of sequence-unrelated members of enzyme superfamilies by activity-based protein profiling. Angew. Chem. Int. Ed. Engl. *44*, 2400–2403.
33. Iacobuzio-Donahue, C.A., Maitra, A., Shen-Ong, G.L., van Heek, T., Ashfaq, R., Meyer, R., Walter, K., Berg, K., Hollingsworth, M.A., Cameron, J.L., et al. (2002). Discovery of novel tumor markers of pancreatic cancer using global gene expression technology. Am. J. Pathol. *160*, 1239–1249.
34. Kato, D., Boatright, K.M., Berger, A.B., Nazif, T., Blum, G., Ryan, C., Chehade, K., Salvensen, G.S., and Bogyo, M. (2005). Activity-based probes that target diverse cysteine protease families. Nat. Chem. Biol. *1*, 33–38.
35. Saghatelian, A., Jessani, N., Joseph, A., Humphrey, M., and Cravatt, B.F. (2004). Activity-based probes for the proteomic profiling of metalloproteases. Proc. Natl. Acad. Sci. USA *101*, 10000–10005.
36. Chan, E.W., Chattopadhaya, S., Panicker, R.C., Huang, X., and Yao, S.Q. (2004). Developing photoactive affinity probes for proteomic profiling: hydroxamate-based probes for metalloproteases. J. Am. Chem. Soc. *126*, 14435–14446.
37. Sieber, S.A., Niessen, S., Hoover, H.S., and Cravatt, B.F. (2006). Proteomic profiling of metalloprotease activities with cocktails of active-site probes. Nat. Chem. Biol. *2*, 274–281.
38. Groll, M., Nazif, T., Huber, R., and Bogyo, M. (2002). Probing structural determinants distal to the site of hydrolysis that control substrate specificity of the 20S proteasome. Chem. Biol. *9*, 655–662.
39. Li, Y.M., Xu, M., Lai, M.T., Huang, Q., Castro, J.L., DiMuzio-Mower, J., Harrison, T., Lellis, C., Nadin, A., Neduvelil, J.G., et al. (2000). Photoactivated γ-secretase inhibitors directed to the active site covalently label presenilin 1. Nature *405*, 689–694.
40. Vocadlo, D.J., and Bertozzi, C.R. (2004). A strategy for functional proteomic analysis of glycosidase activity from cell lysates. Angew. Chem. Int. Ed. Engl. *43*, 5338–5342.
41. Hekmat, O., Kim, Y.W., Williams, S.J., He, S., and Withers, S.G. (2005). Active-site peptide "fingerprinting" of glycosidases in complex mixtures by mass spectrometry. Discovery of a novel retaining β-1,4-glycanase in *Cellulomonas fimi*. J. Biol. Chem. *280*, 35126–35135.
42. Liu, Y., Shreder, K.R., Gai, W., Corral, S., Ferris, D.K., and Rosenblum, J.S. (2005). Wortmannin, a widely used phosphoinositide

3-kinase inhibitor, also potently inhibits mammalian polo-like kinase. Chem. Biol. *12*, 99–107.

43. Yee, M.C., Fas, S.C., Stohlmeyer, M.M., Wandless, T.J., and Cimprich, K.A. (2005). A cell-permeable activity-based probe for protein and lipid kinases. J. Biol. Chem. *280*, 425–437.
44. Barglow, K.T., and Cravatt, B.F. (2004). Discovering disease-associated enzymes by proteome reactivity profiling. Chem. Biol. *11*, 1523–1531.
45. Adam, G.C., Sorensen, E.J., and Cravatt, B.F. (2002). Proteomic profiling of mechanistically distinct enzyme classes using a common chemotype. Nat. Biotechnol. *20*, 805–809.
46. Speers, A.E., and Cravatt, B.F. (2005). A tandem orthogonal proteolysis strategy for high-content chemical proteomics. J. Am. Chem. Soc. *127*, 10018–10019.
47. Kidd, D., Liu, Y., and Cravatt, B.F. (2001). Profiling serine hydrolase activities in complex proteomes. Biochemistry *40*, 4005–4015.
48. Patricelli, M.P., Giang, D.K., Stamp, L.M., and Burbaum, J.J. (2001). Direct visualization of serine hydrolase activities in complex proteome using fluorescent active site-directed probes. Proteomics *1*, 1067–1071.
49. Fuji, M., Watanabe, F., Fujii, Y., Hashizume, H., Okuno, T., Shirahase, K., Teshirogi, I., and Ohtani, M. (1997). A stereoselective and highly practical synthesis of cytosolic phospholipase A2 substrate, 2-S-arachidonoyl-1-O-hexadecyl-sn-2-thioglycero-3-O-phosphocholine. J. Org. Chem. *62*, 6804–6809.
50. Lamant, V., Chap, H., Klaebe, A., Perie, J., and Willson, M. (1987). Synthesis of a thiophospho analogue of platelet activating factor (RS)- and (S)-1-hexadecyl-2-acetylglycero-thiophosphocholine. J. Chem. Soc. Chem. Commun. *21*, 1608–1609.
51. Smith, C.A., Want, E.J., O'Maille, G., Abagyan, R., and Siuzdak, G. (2006). XCMS: processing mass spectrometry data for metabolite profiling using nonlinear peak alignment, matching, and identification. Anal. Chem. *78*, 779–787.
52. Ritter, K. (1991). Affinity purification of antibodies from sera using polyvinylidenedifluoride (PVDF) membranes as coupling matrices for antigens presented by autoantibodies to triosephosphate isomerase. J. Immunol. Methods *137*, 209–215.
53. Jessani, N., Humphrey, M., McDonald, W.H., Niessen, S., Masuda, K., Gangadharan, B., Yates, J.R., III, Mueller, B.M., and Cravatt, B.F. (2004). Carcinoma and stromal enzyme activity profiles associated with breast tumor growth in vivo. Proc. Natl. Acad. Sci. USA *101*, 13756–13761.
54. Tanyi, J.L., Morris, A.J., Wolf, J.K., Fang, X., Hasegawa, Y., Lapushin, R., Auersperg, N., Sigal, Y.J., Newman, R.A., Felix, E.A., et al. (2003). The human lipid phosphate phosphatase-3 decreases the growth, survival, and tumorigenesis of ovarian cancer cells: validation of the lysophosphatidic acid signaling cascade as a target for therapy in ovarian cancer. Cancer Res. *63*, 1073–1082.